Proc. Indian Acad. Sci. (Earth Planet. Sci.), Vol. 102, No. 1, March 1993, pp. 157–173.

The "susceptibility factor" in the atmospheric response to periodic forcing

WILLIAM H CAMPBELL and REID A BRYSON

Center for Climatic Research, Institute for Environmental Studies, University of Wisconsin-Madison, 1225 W. Dayton Street, Madison, Wisconsin 53706, USA

Abstract. Evidence is presented of a periodic component in the inter-annual variability of precipitation and pressure data for India during June, the month of the onset of the Indian southwest monsoon. Two frequencies that explain a statistically significant percent of the variance in these data sets are the same as the two that explain most of the variance of the average monthly lunar tidal potential for June. Not only are the frequencies the same but they are also in phase which strongly suggests that lunar tides in the atmosphere do, in fact, produce an element of climatic variability. The amplitude of the atmospheric response to this periodic forcing was not constant in time but was found to be related to the long term change in northern hemispheric surface temperature. This susceptibility of the atmosphere to an external forcing results in a nonlinear relationship between forcing and response. As a result, nonlinear regression had to be used in order to adequately define the magnitude of the response at a given frequency. The ramifications of this nonlinear response are discussed. The nonlinear interaction of the northern hemisphere temperature and the 18·6 year lunar nodal cycle results in a modulation of the frequency which appears in a linear spectral analysis near 22 years. Thus, the 22-year cycle often found in meteorological data sets may instead be the result of the modulated nodal cycle.

Keywords. Monsoon; lunar effects; spectral analysis.

1. Introduction

No theory of climatic variability based on a single parameter can explain all of the observed inter-annual variance, because the climate is controlled by many factors. Campbell *et al* (1983), hereafter referred to as CBB, presented an hypothesis that one forcing mechanism, lunar atmospheric tides, accounts for a statistically significant percent of the climatic inter-annual variability of June precipitation in northern India. CBB showed that two frequencies dominate the spectrum of average monthly lunar tidal potential for June. The frequency that explained the most variance. (·0537 year^{-1}) was associated with the lunar nodal cycle. The only other spectral peak of any consequence was at a frequency around ·263 year^{-1}. CBB then showed that the monthly June rainfall totals in northern India had a well defined spectral signature with two dominant modes of variation at around ·05 and ·26 year^{-1}.

This paper will present further evidence for the effect of lunar atmospheric tides on the inter-annual variability of both rainfall and surface pressure during the onset of the Indian southwest monsoon. In addition, the concept of modulation of the atmospheric response to periodic external forcing will be applied and given as an explanation for the frequency shift (reported in CBB) observed in the June precipitation data of northern India. In the sections that follow we will refer to the modulation term, which is a function of space and time, as the *susceptibility factor.*

2. General discussion

If one has an hypothesis that some kind of external periodic forcing is acting on the atmosphere, then a typical way of expressing the relationship between forcing and response is:

$$R = k\cos(2\dot{U}ft + \phi) \tag{1}$$

where R is the response of the climatic variable to the forcing, k is the amplitude of the response, $\cos(2\dot{U}ft + \phi)$ represents the periodic forcing, f is the forcing frequency and ϕ is the phase.

The factor k is the amplitude of the response and, therefore, indicates how susceptible the climatic variable is to the forcing. If k is large then the climatic variable is very susceptible to the forcing. In equation (1), k is a constant making this a linear equation; however, considering the nonlinearity of the atmosphere, there is no reason to assume that k is a fixed value. If the atmosphere is more susceptible to the periodic forcing at certain times than at others, then the susceptibility factor, k, is also a function of time and we obtain the nonlinear equation:

$$R = k(t)\cos(2\dot{U}ft + \phi). \tag{2}$$

Even if an external forcing is always acting on the earth-atmosphere-ocean system, equation (2) now implies that the response to that always-present forcing is not necessarily the same at all times. In other words, there is now another variable to consider in determining how the atmosphere responds to the external forcing. It is this variable that modulates the effects of the external forcing at a given location.

For convenience, let us assume that the modulation variable is also periodic but with a much longer period than the forcing. The susceptibility factor can be written as:

$$k(x, y, t) = A[Q(t) - B(x, y)] \tag{3}$$

where $k(x, y, t)$ is the susceptibility factor, $Q(t)$ is the modulating variable and will be called the "susceptibility parameter", A provides the sign and the magnitude of the response and will be called the "susceptibility coefficient" and B is the "susceptibility threshold" to be discussed below.

The susceptibility threshold is written as a function of space, because as we shall see, for a given forcing frequency the value of B varies from station to station.

Since $Q(t)$, in this conceptual model, is assumed to be a cosine function, then its values range between $+1{\cdot}0$ and $-1{\cdot}0$. Therefore, if B equals one and $Q(t)$ is at a positive maximum, the response will be zero. Similarly, the absolute magnitude of the response will be largest when $Q(t)$ is at a negative maximum. If B is less than one, then for a certain period of time, the response actually reverses sign. If B is greater than one then the atmosphere is always susceptible to the forcing but to varying degrees. As B increases the effect of $Q(t)$ diminishes. Thus, if B is large enough, this modulating effect is essentially negligible and only the forcing itself is important.

Figure 1 shows the effect that the susceptibility threshold has. In this example, a forcing frequency of $0{\cdot}20$ year^{-1} and a modulating period of 180 years were used. In all four cases in figure 1 year 20 has relative minimum (negative maximum) in the cycle. However, depending on the value of B, year 90 is either in phase, zero, or 180 degrees out of phase with year 20. Thus, the value of the susceptibility threshold, B, determines how the cosine $Q(t)$ in the equation (3) actually modulates the external

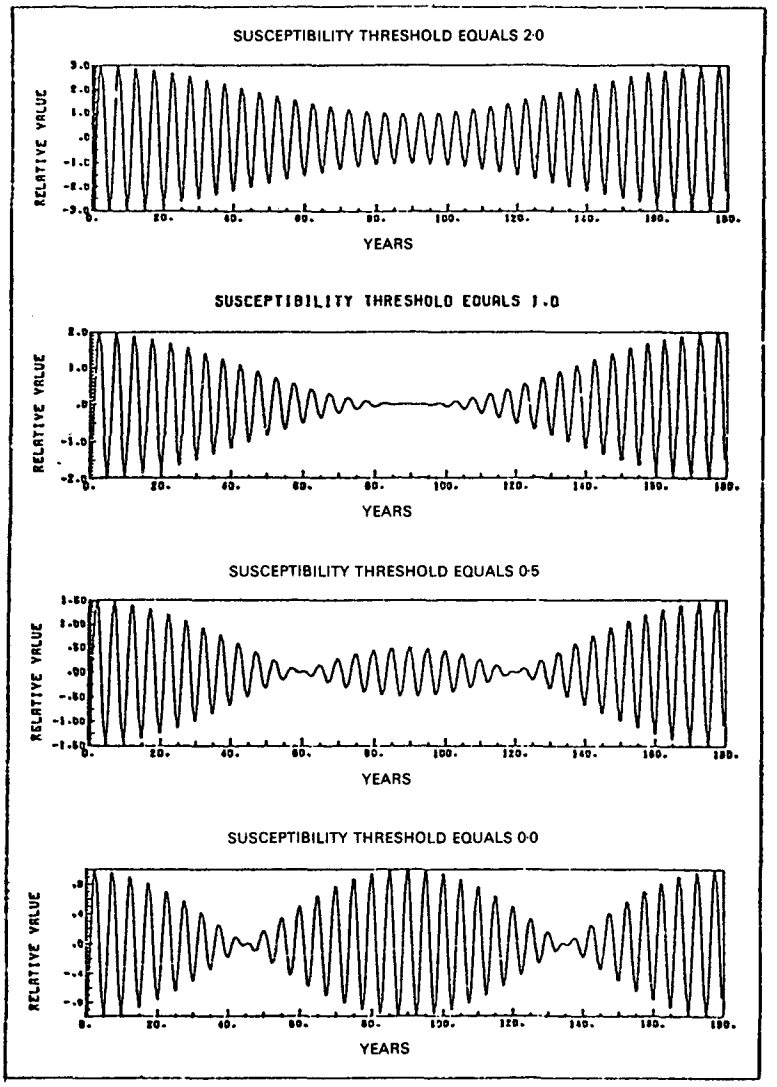

Figure 1. Time series for a response to a forcing with a five-year period and a 180-year modulation. The only difference between each time series is the value of the susceptibility threshold. These plots show how sensitive the response is to the value of the susceptibility threshold in equation (3).

forcing. We will see that the value of the susceptibility threshold has a regional character. Since we currently have little physical basis for determining the value of b, it will be derived empirically from the data.

If the atmosphere responds linearly to a periodic forcing (as in equation (1)) then a spectral analysis will have power at the associated frequency. However, if equation (2) is the appropriate form of the response, then the value of B can have a marked effect on the frequency observed in a spectral analysis of the data. For example, if B is zero then with $Q(t)$ being a cosine, the following relationship applies:

$$A\cos(Mt)\cos(Ft) = A/2[\cos(F-M)t + \cos(F+M)t] \tag{4}$$

where F represents the forcing frequency and M represents the modulating frequency. Thus, in a spectral analysis (which is a linear analysis) neither the frequency F nor the frequency M would appear. Since M has been assumed to be associated with a long period then the effect here is to split the power associated with the frequency F into power at somewhat higher and lower frequencies. B does not have to be zero, however, and the exact nature of the frequency shift is dependent upon the value of B and what portion of the modulating cycle is included in the observed data. If B is greater than one, then there should be no apparent frequency shift, for the periodic signal is always present without a phase shift.

3. Specific example

CBB found that two frequencies dominated the inter-annual variability of June precipitation in northern India. The empirical evidence strongly suggested that these two frequencies were the result of soli-lunar atmospheric tides. These tides are always present in the atmosphere but their effect should be most readily observed in a region that is especially sensitive to a synoptic singularity like the arrival of the monsoon where small departures from the normal arrival date have a large impact on the percent of normal rainfall received during the calendar month of June. Since the pre-monsoon period in northern India is very dry and the average onset date is late in the month of June, the amount of June rainfall received in the region is very sensitive to the timing of the arrival of the monsoon.

CBB only performed a linear analysis of the data, thereby assuming that the amplitude of the periodic component of inter-annual variability was constant. However, in view of the discussion in the preceding section we must now ask if there is any factor which might modulate the effects of the hypothesized external forcing. One such factor might be the intensity of the monsoon circulation. If there is an epoch when the monsoon circulation is stronger than "normal" year after year, then during those years the monsoon would conceivably reach northern India much earlier than it had in prior years. Thus, this region would no longer be as sensitive to the timing of the monsoon arrival for there would now be two to three weeks of rain during the calendar month of June rather than just a few days at the end of the month. As a result, if soli-lunar atmospheric tides are in fact modulating the position of the monsoon front, as put forth in CBB, the periodic signature would no longer be as clear in the data during this epoch. Thus, the strength of the monsoon circulation could have an impact on the susceptibility of northern India to the periodic forcing.

We have chosen hemispheric temperature as the susceptibility parameter, $Q(t)$ in equation (3), for it is one factor which has an important effect on the intensity of the monsoon circulation (Bryson and Swain 1981; Kutzbach and Otto-Bliesner 1982). Hemispherically warm periods produce strong monsoons; whereas, cold periods have more winter-like circulation patterns with weak monsoon circulations. Therefore, if we assume that the susceptibility factor is dependent on the strength of the monsoon circulation, then making it a function of northern hemisphere temperature seems to be an appropriate approximation.

One source of data for computation of a susceptibility factor based on northern hemispheric temperature is found in Jones *et al* (1982). They published a 100 year time series of mean monthly and annual northern hemispheric temperatures. While

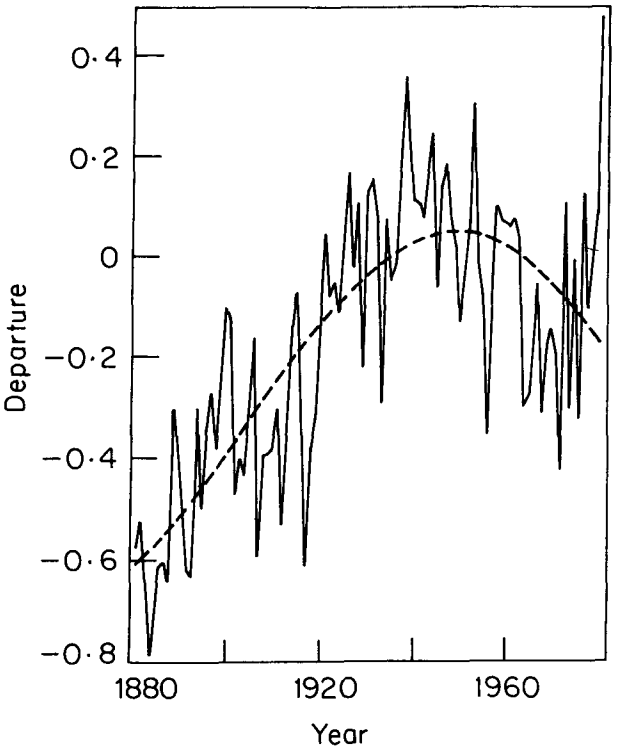

Figure 2. The solid line is the northern hemisphere annual mean surface temperature anomalies from the 1946–1960 mean (after Jones *et al* 1982). The dashed line is the best fitting cosine (explaining 58 percent of the variance) used in the susceptibility factor.

there are difficulties with any such data set, the long term characteristics of northern hemispheric temperature may be determined. Figure 2 shows the mean annual northern hemisphere surface temperature anomalies from Jones *et al* (1982). A definite warming trend into the 1940s and then cooling into the 1970s is observed. As a first approximation to this temperature data, the best fitting cosine curve was found to have a period of about 172·6 years with maximum value occurring in the year 1948. This curve, shown as the dashed curve in figure 2, explains 58 percent of the variance of the mean annual northern hemisphere surface temperature time series. Looking at the time series of average temperature for the months April through July (i.e., around the time of the monsoon onset) the best fitting cosine is very similar to the one for the annual data.

Making $Q(t)$ equal to the cosine approximation of the northern hemisphere surface temperature then provides an experimental form of the susceptibility parameter. It must be emphasized that the resulting form of the susceptibility factor should be raised to some power. Further research will be required to gain greater insight into the characteristics of this nonlinear factor.

To test the hypothesis of atmospheric susceptibility to external forcing, nonlinear regression was used on monthly (June) time series of pressure and precipitation at stations in India and Pakistan. The regression equation was:

$$P = A[\cos(2\dot{U}f_1 t + \phi_1) - B]\cos(2\dot{U}f_2 t + \phi_2) + C \tag{5}$$

where P is the value of the climatic element (e.g., precipitation or station pressure) predicted by the regression; A provides a magnitude and sign for the response and is a parameter of the regression; f_1, ϕ_1 are the fixed frequency and phase of the cosine which best fits the northern hemisphere temperature time series, B is the susceptibility threshold and is a parameter of the regression; f_2 is the forcing frequency (·053725 year^{-1}), ϕ_2 is the phase of the forcing and is a parameter of the regression, C is the mean of P.

The forcing frequency, ·053725 year $^{-1}$, is related to the 18·6 year lunar nodal cycle and is one of the two frequencies discussed in CBB.

The nonlinear regression routine returns the values for the three parameters (A, B, and ϕ_2) along with the mean, C. The susceptibility threshold B is not fixed in the regression so that we may see how sensitive the particular climatic variable is to the effects of hemispheric warming and cooling at a given station. The phase of the forcing cosine, ϕ_2, is allowed to float to test whether or not the climatic variable response is, in fact, in phase with the hypothesized lunar forcing.

Let us first consider the normalized June cube rooted precipitation data (1895–1975) for one particular station, Sagar (WMO number 426710 at 23·9°N, 78·8°E). Figure 3 (top) shows the predicted values from a straight linear regression against the nodal cycle (solid line) and the predicted values of the response from the nonlinear regression using equation 5. The nonlinear regression anomaly equation for Sagar is:

$$P = -1{\cdot}56[Q(t) - 0{\cdot}676]\cos(2\dot{U}ft + 0{\cdot}186) \tag{6}$$

with $t = 0$ in 1895. The percent of the variance explained by the linear regression is 3·6 and by the nonlinear regression is 14·8. To be significant at the 95 percent level the three parameter nonlinear regression equation must explain 9·6 percent of the variance; whereas the two parameter linear regression model must explain at least 7·4 percent. The maximum anomaly attainable for the linear model is 0·18 standard deviations.

In order to compare this empirical response to one predicted by lunar tidal forcing we must first know the phasing of the lunar nodal cycle. As discussed in CBB, the lunar nodal cycle explains by far the largest percent (greater than 90 percent) of the inter-annual variance of a time series of monthly mean tidal potential. The nodal cycle 18·6 years is the time it takes the pole of the moon's orbit to rotate about that of the ecliptic. Since the moon's orbital plane is inclined to the ecliptic at an average angle of 5°9′, the latitudinal range over which the moon traverses during a lunar month varies with an 18·6 year period. The maximum monthly average value of the lunar tidal potential occurs when the latitudinal range is 18·3°N to 18·3°S. The dates of these occurrences are very well established. For example, the maxima in the recent past have occurred on October 20·3, 1894; June 1·7, 1913; January 12·1, 1932; August 23·0, 1950; and April 3·4, 1969 (taken from Wood 1976).

Figure 3 (middle) shows the predicted response (solid line) based on the concept of atmospheric susceptibility to the lunar forcing. It is calculated by using the known phase of the lunar nodal cycle and the empirically determined values of the susceptibility threshold and coefficient in equation 5. As indicated earlier these empirical values are being used since, at the present time, we have no physical basis upon which to determine the susceptibility factor. Also shown in this figure is the unmodulated nodal cycle (dashed line). This curve is shown for phasing information only and the amplitude of the curve has no physical meaning. With the susceptibility

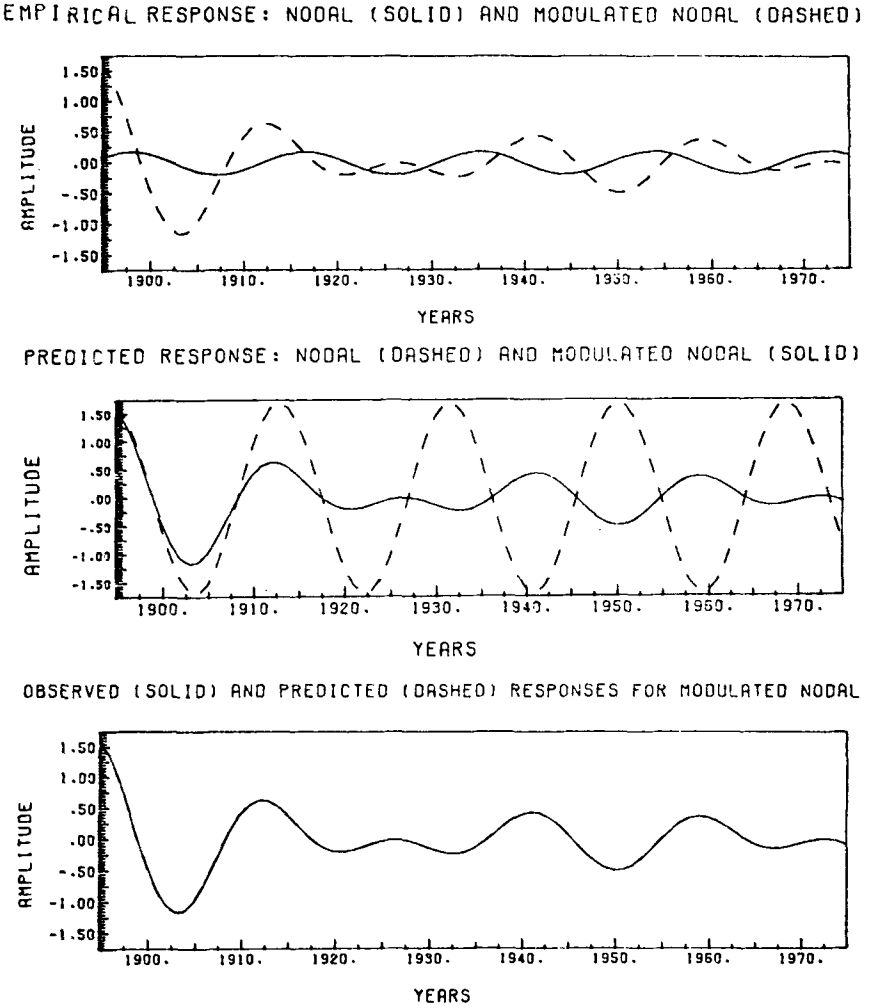

Figure 3. Top. Solid curve is the result of a linear regression of June cube rooted precipitation (normalized) for the years 1895–1975 against a cosine with frequency $\cdot 0537^{-1}$. Dashed curve is the result of a nonlinear regression of the same data using equation (5). Units are standard deviations.

Middle. Solid curve is a time series generated by using equation (5) where the phase, ϕ_2, is defined by lunar orbital mechanics and the parameters A and B are empirically determined values from the regression of Sagar precipitation data using equation (5). Dashed curve provides phasing information for the lunar model cycle. The amplitude has no significance. Units are standard deviations.

Bottom. Superposition of the dashed curve from the top figure and the solid curve from the middle figure. The fit is so close that the dashed curve cannot be seen.

threshold value less than one (i.e., 0·676 in equation 6), the response changes sign so that at the beginning of the record the predicted response is in phase with the nodal cycle but at the end of the record the two curves are out of phase.

The only difference between the predicted and the empirical response of the modulated nodal cycle is the phase of the forcing cosine. In the empirical response,

as stated earlier, the phase is a parameter of the nonlinear regression. In the predicted response the phase is derived from the known orbital mechanics of the moon. Figure 3 (bottom) shows the superposition of these two curves. We see that the empirical response is exactly in phase with the predicted response which is based on lunar forcing and the atmospheric susceptibility to that forcing.

Because of the phase reversal, easily seen in figure 3 (middle), when the precipitation data are regressed linearly against the nodal cycle a statistically insignificant signal is observed with phasing that does not coincide with the lunar nodal cycle. Only after the nonlinear susceptibility factor is applied to the forcing cosine does a significant signal appear at the nodal frequency.

The only climatic variable discussed in CBB was precipitation. However, surface pressure is another important variable with a pattern associated with the onset of the monsoon. Applying the model of equation 5 to surface pressure data for 40

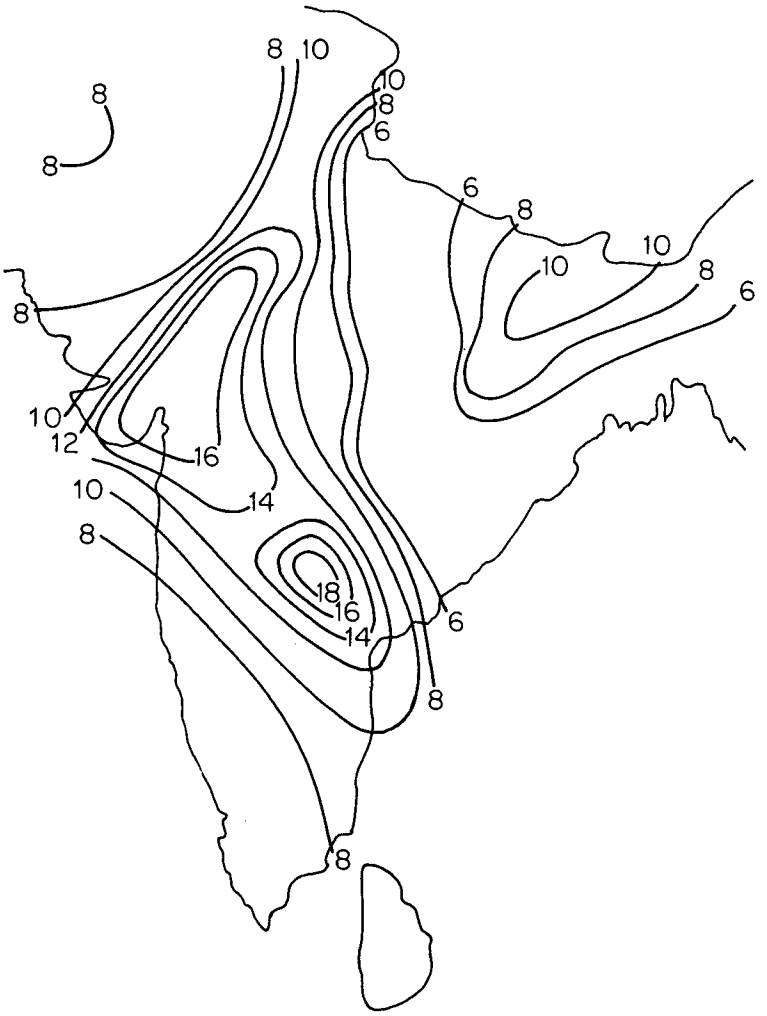

Figure 4. The percent of the station pressure variance explained by using equation (5) (units are percent).

stations in India and Pakistan (1895, through 1960) produced the percent variance and the susceptibility threshold, B, mapped in figures 4 and 5, respectively.

The surface pressure anomaly maps for the years 1895, 1903, 1913, and 1922 are shown in figure 6. These years were chosen because they are the Junes that are at the extremes of the predicted response at the nodal cycle. There was a maximum in the predicted response in 1894; however, since the data set began in 1895, that year was used. Also, the other years are not necessarily a maximum or minimum in the lunar nodal cycle but may be a year off because of the effect of the amplitude modulation. In 1895 and again in 1913, a large positive anomaly dominated northeastern India, extending northwestward along the Himalayas, whereas a large negative anomaly occurred over western India. In the years 1903 and 1922 the reverse pattern occurred. We have postulated that the tidal effects are less important in warmer years and we see that the magnitude of the anomalies decreases from 1895 to 1922—a period of warming in the cosine approximation to the northern hemisphere temperatures. The axis of the reversing pattern lies just about along the average position of the

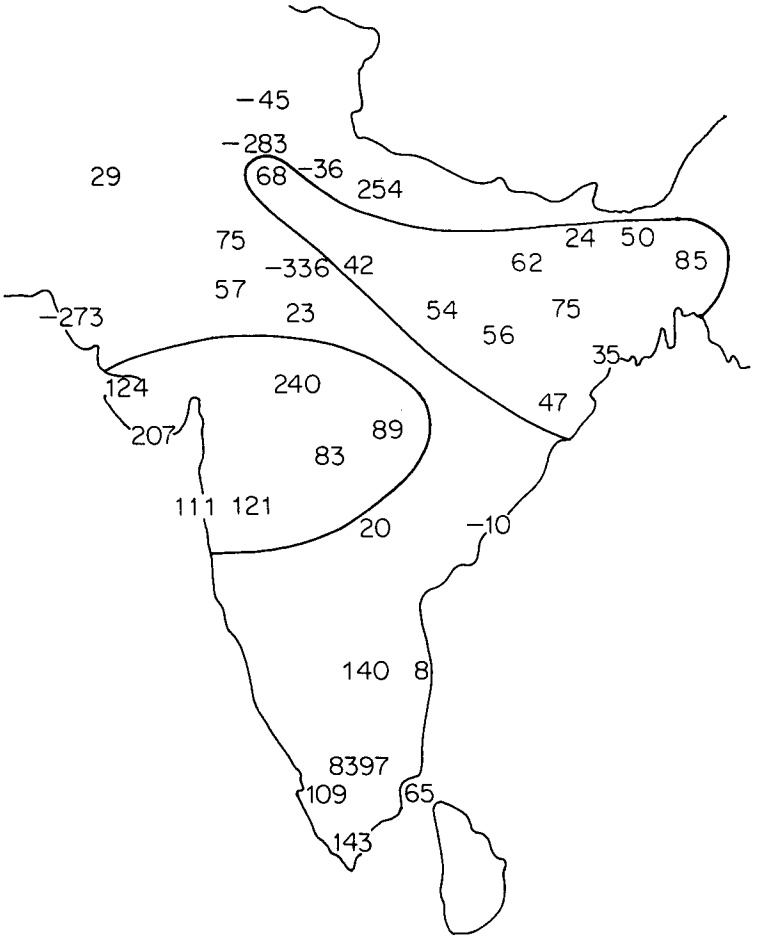

Figure 5. The value of the susceptibility threshold from the regression of the station pressure data by using equation (5) (units are value $\times 10^{-2}$). The two areas outlined show that the threshold values are different in northeastern India from what they are in western India.

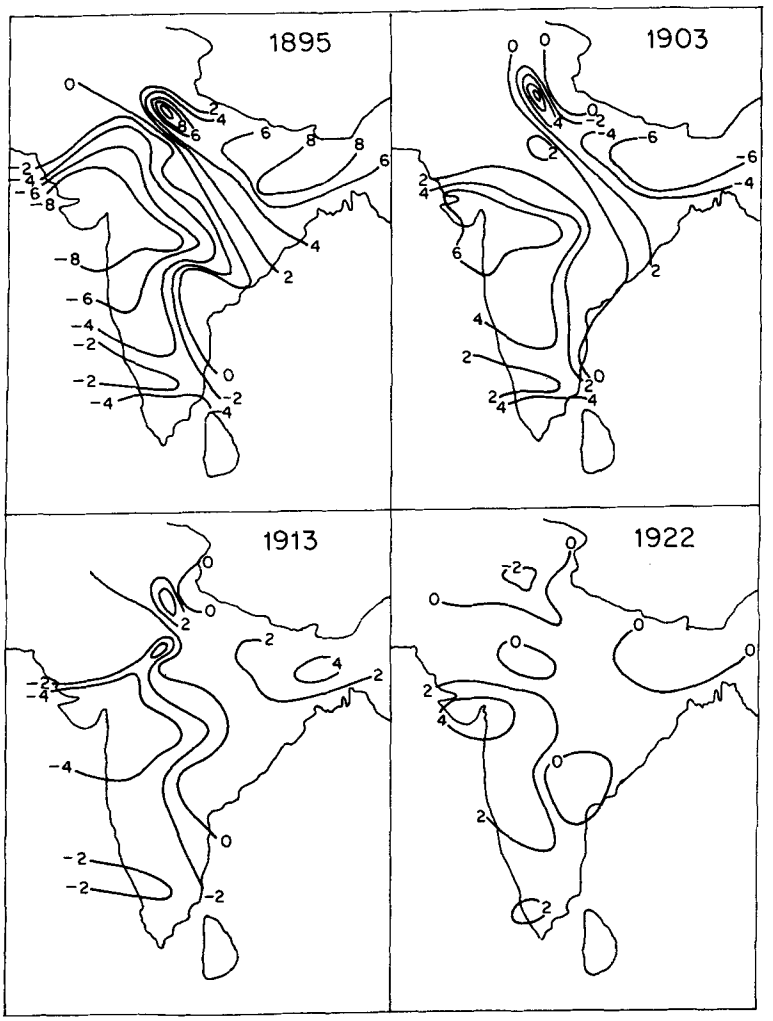

Figure 6. Anomaly maps of station pressure for the years indicated using equation (5) (units are mb $\times 10^{-1}$).

monsoon trough in June with the anomaly center to the north of this axis lying along the Himalayas. The standard deviation for June monthly mean station pressure over most of India is of the order of 1 mb; therefore, in 1895, for example, the anomalies are about one standard deviation.

Looking at the susceptibility threshold values of figure 5 we see that the susceptibility threshold is greater than one for most of the stations of interest in the west while it is less than one in the northeast. No attempt has been made to analyze these data, since the values vary so much. The fact that the susceptibility threshold is less than one in northeastern India means that once the temperature cosine reaches that value (on its way to a maximum of one at the warmest part of the cycle) the sign of the nodal forcing cosine reverses. Thus, where the signs of the pressure anomalies in the northeast and in the west were opposite in the early part of the record, they become the same as the hemisphere warms. This greatly decreases the

NE/SW pressure gradient making the overall response at the nodal forcing frequency close to zero.

In order to establish the phasing of this periodic oscillation in the pressure data, let us examine the average pressure anomaly of the following seven western stations and eight northeastern stations:

WEST—WMO	NORTH—WMO
42731—Dwarka	42261—Agra
42909—Veraval	42475—Allahabad
43057—Bombay	42587—Daltonganj
43063—Pune	42970—Cuttack
42933—Akola	42807—Calcutta
42754—Indore	42599—Dumka
42876—Nagpur	42391—Darbhanga
	42099—Ludhiana

The difference between the two averages (North minus West) will provide a measure of the strength of the NE/SW pressure gradient. The difference was calculated so that it would be negative for dry years. Table 1 provides a comparison of this difference for the years surrounding the maximum effect of the predicted response (i.e., the empirically determined susceptibility factor times the lunar forcing cosine). One notes that the pressure anomaly difference is, in fact, strongest at the beginning of the data record which is well into the coldest period of the best fit northern hemisphere cosine curve. Thus, the actual atmospheric response is much stronger when the hemisphere is coldest. Also, the year of the maximum pressure anomaly difference agrees with the year of the maximum predicted response and the correlation of the 66 year time series of the regressed pressure anomaly difference and the predicted response is $-\cdot 972$ when using a susceptibility threshold of $\cdot 94$ which is the average value for the 15 stations used. The minus sign of the correlation is a result of the way the difference in anomalies was calculated. Thus, the actual atmospheric response is very much in phase with the predicted response.

A periodogram of the entire 66 year pressure anomaly difference time series (a portion of which is given in table 1 is shown in figure 7. The most important point to note is that even though the regression equation (equation 5) explicitly defined the frequency to be $\cdot 053725\,\text{year}^{-1}$. This frequency shift (line splitting) is due to the nonlinearity induced by the susceptibility factor. A similar type of frequency shift due to the modulation of the nodal cycle is also observed in the regressed time series for Sagar June precipitation discussed earlier.

A physically consistent synoptic climatology can be derived from figures 3 and 6. Bhalme and Mooley (1980) in a study of the seasonal surface pressure anomalies during drought and flood years, found strikingly similar patterns to those presented in figure 6. They were not dealing with any periodic component of the data in their analysis but with the total variability for the entire monsoon season. The magnitudes of their west coast departures ($-0{\cdot}6$ mb to $+0{\cdot}8$ mb) are comparable to the magnitude of the anomalies from this periodic model ($-1{\cdot}0$ mb to $+0{\cdot}8$ mb). This indicates that certainly some of the variance associated with drought and flood years is associated with this periodic component of the variability. Research (e.g., Raghavan

Table 1. Pressure anomaly difference compared to the predicted response.

Year	Pressure anomaly difference (mb)	Predicted response threshold ($B = 0{\cdot}94$) (relative numbers) $\times 10^{-2}$
1895	1·38	−1·29
1896	1·16	−1·10
1902	−0·96	0·90
1903	−1·07	1·01
1904	−1·04	0·99
1905	−0·91	0·87
1911	0·57	−0·58
1912	0·66	−0·67
1913	0·67	−0·68
1914	0·61	−0·60
1921	−0·29	0·37
1922	−0·31	0·38
1923	−0·30	0·34
1924	−0·27	0·27

Note. The pressure anomaly difference is calculated by taking the difference of the average anomaly for 8 northeastern stations and seven western stations. The predicted response uses the average susceptibility threshold for the 15 stations.

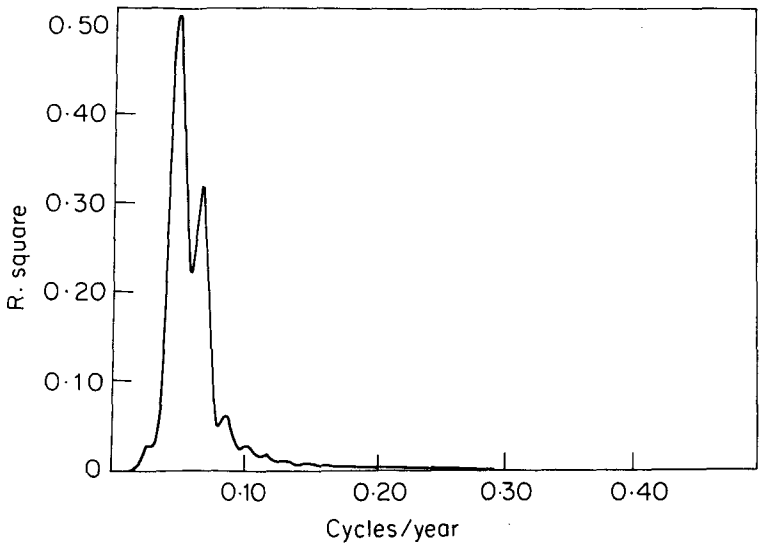

Figure 7. A periodogram analysis of the pressure anomaly difference time series (1895–1960).

1973) has shown that when the pressure anomaly along the Himalayas is negative, as it was in 1903, breaks occur in the monsoon. At the same time there is a large positive anomaly on the west coast which decreases the strength of the southwesterly monsoon current. These anomaly centers create a strong NE/SW pressure gradient

anomaly across the Gangetic Plain of India so that for 1903 the calculated anomalous geostrophic flow is directed from the dry deserts of northwest India and Pakistan onto Central India adding further to the dryness that has already been discussed in conjunction with this pattern. Sagar lies in the region of this pressure gradient and we see from figure 3 that June 1903 was a very dry month whereas June 1895, when pressure anomaly pattern was reversed, was a wet month.

Using the methodology presented in this section we are now in a position to better explain the origin of the two frequencies (·0482 year^{-1} and ·262 year^{-1}) observed in the periodogram of the coefficient time series of the first eigenvector of June precipitation discussed in CBB and reproduced here as figure 8. If we calculate a time series of monthly mean lunar tidal potential for June (1899–1960), we get the periodogram shown in figure 9a with a large peak at ·053 year^{-1} (over 95 percent of the variance) and a much smaller peak at ·263 year^{-1} (4 percent of the variance). Thus, this tidal potential time series is very well represented by the summation of two cosines with these frequencies. To calculate the predicted response based on the hypothesis of atmospheric susceptibility to lunar forcing, a susceptibility factor was applied to each cosine where the susceptibility parameter was the cosine fit to the northern hemisphere temperature data, the susceptibility coefficient was the amplitude of the cosine from the original lunar tidal potential time series and the susceptibility threshold was a representative, empirically determined value. There is no reason to assume that the susceptibility threshold is the same for both frequencies and, in fact, our analysis showed that the value for the response at ·263 year^{-1} was typically greater than one whereas the value for the response at ·0537 year^{-1} was less than one. Using susceptibility threshold values of 1·8 for 0·263 year^{-1} and 0·93 for 0·0537 year^{-1} produced a predicted response time series which had the spectral characteristics

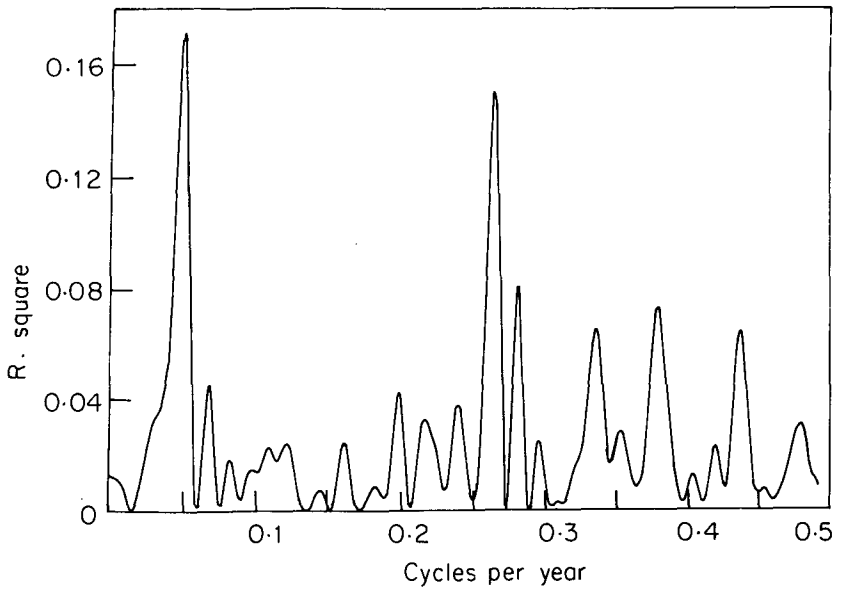

Figure 8. A periodogram of the coefficients of the first eigen vector of June cube rooted precipitation (1895–1975). The two dominant peaks are at ·0482 year^{-1} and ·262 year^{-1}. Reproduced from Campbell *et al* (1983).

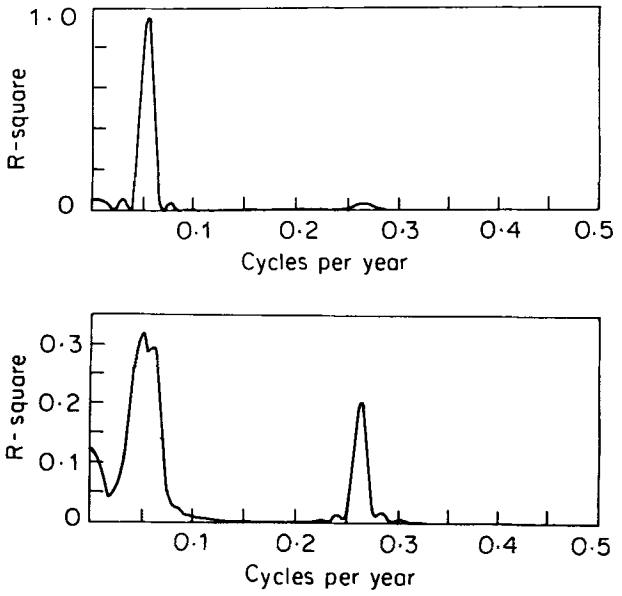

Figure 9. Periodograms of the lunar tidal potential and the associated predicted response for the years 1899 through 1960. The predicted response time series was calculated using the amplitudes and phases for the frequencies ·0537 year^{-1} and ·263 year^{-1} from the lunar tidal potential time series along with the representative values of the susceptibility threshold.

shown in figure 9b with the peaks at ·0484 year^{-1} and ·263 year^{-1} explaining 32·2 and 20·6 percent of the predicted response variance, respectively. There are several important points to note:

a. The peak at the nodal cycle no longer exists but has shifted to the lower frequency of ·0484 year^{-1} and its amplitude has decreased with an indication of band splitting. This is the result of the amplitude modulation.
b. When a representative value for B is used for both lunar frequencies, even though in the lunar potential time series the amplitude of ·263 year^{-1} is considerably less than the amplitude of the nodal (see figure 9a), the spectral characteristics of the predicted response no longer reflect this difference but instead the amplitudes of the two frequencies are fairly close.
c. The peak at ·263 year^{-1} is not shifted. It exists in both the forcing and the predicted response.

In a footnote added in proof in CBB the authors stated that "the two frequencies observed in the precipitation data can be obtained if the two postulated soli-lunar forcing frequencies are modulated by a long-term fluctuation arising from a source other than the orbital characteristics of the earth–moon–sun system." This footnote was added because the research discussed above appears to indicate that the two peaks of figure 8 can now be explained in terms of the effects of lunar tidal forcing on the atmosphere being modulated by the intensity of the monsoon which is represented by northern hemisphere surface temperature in this experimental model.

4. Possible alternative to the sunspot cycle

Bhalme and Mooley (1981) studied cyclic variations in the Flood Area Index (FAI) for India (see figure 10 for FAI|1 and FAI|2 time series) and concluded that there is strong statistical evidence for the relationship between the double sunspot cycle and the areal extent of flooding over India, for their spectral analyses had a peak at band 4 (·0455 year^{-1} which is a 22 year period). This frequency contained 12 percent of the variance for FAI|1 and 16 percent for FAI|2. We have read the values of the index directly from their published figure. A periodogram analysis (which provided tenth band resolution) showed that the spectral peak was at a slightly higher frequency that their harmonic analysis could resolve. The spectral peaks of the periodogram analysis are given in table 2. The spectral peak for the FAI|1 time series was about ·048 year^{-1} which is close to the frequency found in the linear eigenvector analysis of June precipitation. The spectral peak for the FAI|2 time series was about ·047 year^{-1} which is close to the frequency found in figure 8. Also, the percent variances explained by a 22 year period in our analysis were 14·7 and 21·0 for FAI|1 and FAI|2, respectively, compared to the 12 percent and 16 percent reported by Bhalme and Mooley.

In addition to the FAI time series, figure 10 also has superimposed a dashed curve which is the result of the regression of the data against a 22 year period, representing

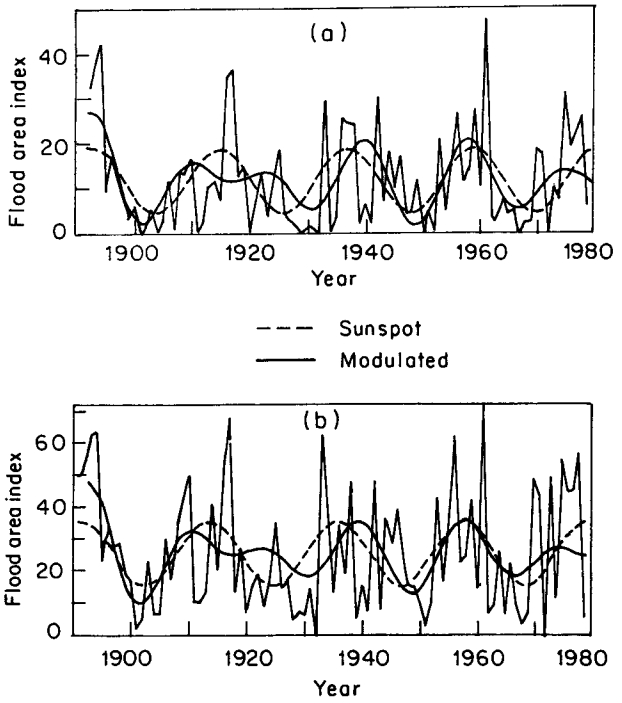

Figure 10. Flood Area Index time series for the indicated flood intensities (after Bhalme and Mooley 1980). The dashed curves represent the predicted values of a regression of these data against the 22 year double sunspot cycle, while the solid curves represent the predicted values of a regression of these data using equation (5). Values read directly from the published figure.

Table 2. Results of a periodogram analysis.

Time series	Spectral Peak period	Percent Variance	
FAI|1	·0477 yr^{-1}	20·95 yr	16·4
FAI|2	·0466	21·46	22·0

the double sunspot cycle, and a solid curve which is the result of regression of the data using equation (5). Note that the solid curve provides the largest anomalies and also that the two curves are nearly in phase during much of the period of time covered by the data set.

When the two FAI indices were regressed against the model given in equation (5), the FAI|1 regression explained 17·8 percent of the variance compared to the 14·7 percent for the double sunspot cycle from our periodogram analysis. The respective percents for the FAI|2 regression were 26·9 and 21·0. One would expect the nonlinear regression model to explain somewhat more of the variance since it has three parameters whereas the harmonic analysis only has two. To be significant at the 99 percent level, a two parameter linear regression model must explain 10·3 percent of the variance and a three parameter model must explain 12·6 percent indicating that both hypotheses produce statistically significant results. However, the modulated nodal cycle provides a better fit to the data and it represents physically known phenomena. Thus, the modulated nodal cycle provides an alternative explanation for the variability which appears to have about a 22 year period in a spectral analysis.

5. Conclusions

Building on the results of CBB, further empirical evidence has been presented supporting the hypothesis that lunar atmospheric tides do have an effect on the climate. The periodic signature is observable in mean monthly climatic data from regions that are especially sensitive to a synoptic singularity like the onset of the monsoon. We have shown that the two dominant frequencies found in the precipitation records of northern India (as reported in CBB) are the same two frequencies that explain almost 100 percent of the inter-annual variability of montly mean lunar tidal potential. Not only are the response and forcing frequencies the same but they are also in phase which strongly suggests that lunar tides in the atmosphere do, in fact, produce an element of climatic variability.

An important result of this research is the demonstration that the amplitude of the response to an external forcing is not always constant in time. A trend in the amplitude was found and related to the northern hemisphere surface temperature. This has some important ramifications. First, the trend and periodic components of climatic variability cannot always be treated separately. In the case presented in this paper they are inseparable. At Sagar the forcing frequency was not observable until the amplitude modulation was incorporated into the regression model which then produced a statistically significant and physically meaningful result where the empirical response was exactly in phase with the response predicted by lunar tidal

theory. Second, as a corollary, the assumption of a linear response may obscure a very strong relationship between forcing and response because the nonlinear modulation may suppress the variance at the forcing frequency and shift it to a lower frequency in a linear spectral analysis.

Acknowledgements

The authors are indebted to Pat Behling for development of the data base used in this research. Major W.H. Campbell worked at the University of Wisconsin-Madison under the Air Force Institute of Technology program.

References

Bhalme H N and Mooley D A 1980 Large-scale droughts/floods and monsoon circulation; *Mon. Weather Rev.* **108** 1197–1211

Bhalme H N and Mooley D A 1981 Cyclic fluctuations in the flood area and relationship with the double (Hale) sunspot cycle; *J. Appl. Meteorol.* **20** 1041–1048

Bryson R A and Swain A M 1981 Holocene variations of monsoon rainfall in Rajasthan; *Quart. Res.* **16** 135–145

Campbell W H, Blechman J B and Bryson R A 1983 Long-period tidal forcing of Indian monsoon rainfall: An hypothesis; *J. Clim. Appl. Meteorol.* **22** 287–296

Jones P D, Wigley T M L and Kelly P M 1982 Variations in surface air temperatures: Part 1. Northern Hemisphere, 1881–1980; *Mon. Weather Rev.* **110** 59–70

Kutzbach J E and Otto-Bliesner B L 1982 The sensitivity of the African-Asian monsoonal climate to orbital parameter changes for 9000 Years B.P. in a low-resolution general circulation model; *J. Atm. Sci.* **39** 1177–1188

Raghavan K 1973 Break-monsoon over India; *Mon. Weather Rev.* **101** 33–43

Wood Fergus J 1976 *The Strategic Role of Perigean Spring Tides* U.S. Department of Commerce, National Oceanic and Atmospheric Administration, Washington, D.C., pp 538